JURNAL POLIMESIN
Unit Penelitian dan Pengabdian Kepada Masyarakat (P2M)
Politeknik Negeri Lhokseumawe
ISSN Print: 1693-5462, ISSN Online: 2549-1199
Website: http://e-jurnal.pnl.ac.id/index.php/polimesin

The influence of height on the spreading distance of axisymmetric jets impinging on a rigid surface

Luthfi*
Mechanical Engineering Department, Politeknik Negeri Lhokseumawe,
Lhokseumawe, 24301, Indonesia
***Email:** luthfi@pnl.ac.id

Abstract

The influence of the domain height of negative buoyancy jets when impinging on a rigid surface has been investigated. The study was conducted numerically by applying the Computational Fluid Dynamics (CFD) method. The numerical model consists of a set of Navier-Stokes equations together with an energy equation. The jet flow was modeled in a two-dimensional axisymmetric coordinate. The governing equations were solved in transient using the finite volume approach. The programming code for the numerical model was written in Fortran. The numerical simulations were run at Froude number Fr = 5.0; Reynolds number, Re = 200 and Prandtl number Pr = 7.0. The investigated parameter, the domain height was varied at around $8.8 \leq H/X_0 \leq 10.2$. The flow visualization created from simulation results has revealed the mystery behind the complex flow behavior in detail. Starting from the initial flow when the jet entered the domain to the complex flow pattern of the jet flow detaching from the top surface. Including when the downflow mixes with the upflow creating a recirculation area near the top surface and the bottom of the domain. The plot of the spreading distance over time shows that there is a maximum distance when the jet starts detaching from the top surface. Gradually, the distance decreases until reaching a fixed final distance when the jet flow reaches quasi-steady. The influence of the domain height that was investigated shows different flow patterns at different heights. The plot of final distances over the domain height shows that there is a nonlinear relationship. The regression equation created from the numerical data shows good agreement and accuracy.

Keywords: impinging jet; transient simulation; computational fluid dynamics; buoyancy and domain height.

1. Introduction

Negative buoyancy jets have long been studied and have had many practical applications in science and engineering. So as negative jets impinging on a rigid surface that are often found in many industrial applications [1]-[9].

Bloomfield and Kerr studied turbulent negative jets in stratification environments numerically and experimentally and they found various equations that could predict negative buoyancy jets behavior [1]. They also used analytical methods to propose theoretical models for turbulent negative buoyancy jets [2].

Lin and Armfield investigated weak negative jets in stratification environments [3] by using two-dimensional axisymmetric computational fluid dynamics (CFD) simulation and they made equations that can predict the jet heights. They did the same study with the same method and got a similar jet height equation but it was for weak negative jets in a homogen environment [4]. Lin and Armfield then took advantage of the superiority of CFD methods to expand their research in studying the characteristics of weak negative jets in more depth, such as the effects of Reynolds and Prandtl numbers [5]; the behavior of negative jets in Reynolds and Froude [6]; and the unsteady character of negative jets [7]. They figured out that for weak negative buoyancy jets, there were some other factors that influence negative jets in addition to that of jets in turbulent conditions. Wiliamson et al. also used CFD methods to study weak negative buoyancy jet behavior [8] and turbulent jet behavior [9]. They found similar equations with the previous studies and succeeded in showing tri-dimensional behavior from negative buoyancy jet in more detail and comprehensive.

A schematic illustration of how the negative buoyancy jets work based on various literature studies is shown in Figure 1 [4].

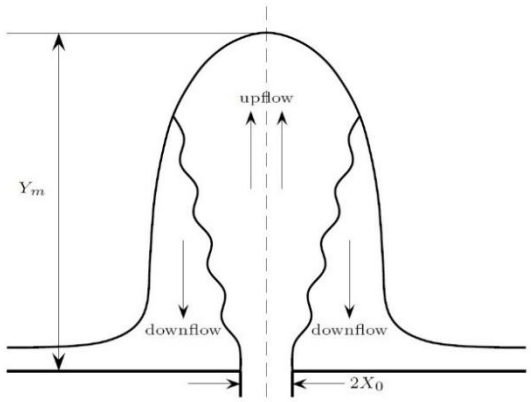

Figure 1. The Illustration of negative jet buoyancy pattern (Self-drawing based on an illustration from Lin and Armfield [4])

The evolution of a negative buoyancy jet when it is injected into a homogen ambient as illustrated in the figure above can be explained as follows. A jet

with certain amount of momentum and with heavier density $\rho_i > \rho_0$ (kg/m3) enters the environmental density ρ_0 (kg/m^3) in vertical direction opposite to gravity. The velocity and momentum of the jet buoyancy is also called upflow or upstream that decreases slowly because of negative buoyancy from the heavier fluid of the environment. As a result, at the previous height Y_m (m) the jet will stop raising and fall down mixed with the fluid around. The falling jet buoyancy is called the downflow and it will gradually decrease the height of the falling jet to Y_f (m).

For turbulent jet, the height is only a function of Froude number (Fr) as written in equation (1) [1,2,8,9]

$$\frac{Y_m}{X_0} = C\ Fr \tag{1}$$

In which X_0 is the inlet radius of the jet (m) and C is the constant that is determined experimentally or numerically. The Froude number (Fr) used in the negative jet as written in the equation (1) is defined as follow,

$$Fr = \frac{V_0}{\sqrt{X_0\ g_0'}} \tag{2}$$

In which V_0 is the jet upstream velocity at its source, that is inlet (m/s) and X_0 is inlet radius (m) and g'_0 is gravitational constant which is reduced due to the density difference between the jet buoyancy and the ambient fluid (m/s^2).

Bloomfield dan Kerr [1,2] studied turbulent negative jet experimentally and numerically using Morton *entrainment* equation to predict the negative jet height as a function of momentum and buoyancy force. Their experimental studies were performed in both homogenous and stratification environments in which the density variation was formed using NaCl solution. The solution was placed on double transparent containers to make better view of the flow observation. The observation of buoyancy patterns was conducted by using a *shadowgraph*. The measured jet height using this method only has an error value of 2-5 %.

Lin and Armfield [3]-[7] studied weak negative jets numerically by solving Navier-Stokes equations directly and they found that the height of the jet was not only a function of Fr but also Re. They modify the equation (1) into,

$$\frac{Y_m}{X_0} = C\ Fr\ Re^a \tag{3}$$

where C and a are the constants found numerically. The Reynolds number used was defined as follow,

$$Re = \frac{V_0\ X_0}{\upsilon} \tag{4}$$

where υ is the kinematic viscosity of the jet fluid entering the domain (m^2/s).

After numerous studies on spreading negative jet were done, the study of impinging negative jet started arising [10]-[14]. Kuruppu and Lemckert have studied *impinging* negative jet experimentally by pumping tap water vertically against gravitational direction to the air until it hit acrylic glass surface [10]. They suggested equations that could estimate the spreading distance as a function of Fr number and proposed relevant coefficient for the impinging jet studied. Holstein and Lemckert studied the impinging negative jet experimentally by injected the air into a container filled with salt from the above until the jet stream impinged the base of the container [11]. They suggested different equations in which not only Fr number but also the height of the domain H had to be included to measure the distance of the spreading jet from the domain base. Lemckert then continued his research in more detail using salt solution injected to a container filled with fresh water from the base of the container until it impinged the surface of the container [12,13]. Based on the range of Re number used and the idea that spreading distance was only influenced by merely the Fr number, Cooper and Hunt also obtained similar results when they studied impinging turbulent negative jet with a relatively high Re number of [14]. They also used salt solution which was injected to a container filled with the fresh water from the base of the container until it hit the top surface of the container. The equations they suggested were simpler than others.

The example applications of impinging jet with negative buoyancy force which are commonly found are the flow mixture of the shielding gas and the welding smoke in GMAW welding, the flow of hot air stream from vertically taken-off airplane or the air flow distribution from the heating system in a very large room [13]. The illustration of impinging the negative jet pattern can be seen in Figure 2.

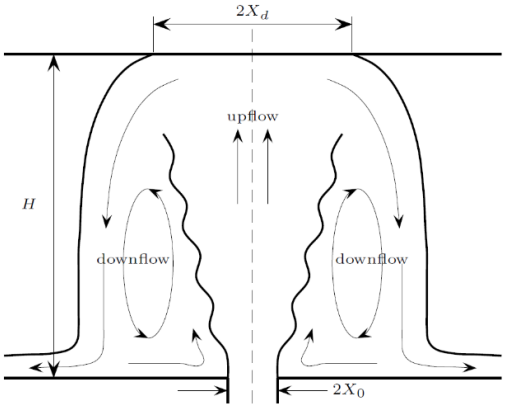

Figure 2. The illustration of impinging negative jet flow (This is drawn based on an illustration from Lemckert [12])

The illustration of how an impinging negative jet works is shown in Figure 2 which is similar to a common negative jet. However, before the jet reaches its maximum height, the flow has already reached a surface and it moves and spread in the impinging surface until a distance X_d, after which the stream falls down forming a downstream flow.

Unlike common negative jets, the study of impinging negative jets has not been much done yet therefore there is little information available in the literature. This led to a high variation of correlation equation [10]-[14]. Lemckert and his colleagues [10]-[13] have investigated impinging turbulent negative jets intensively through some experiments. They found that total distance of impinging jets before it started detaching from the surface, $H+X_d$ (m) was a function of Fr as written in the following equation,

$$\frac{H+X_d}{X_0} = CFr^n \quad (5)$$

where X_0 is the inlet radius (m), C and n are the constants determined empirically by experimental data.

The literature review on the previous study of impinging negative jet shows that the spreading distance X_d was a function of Fr number only. Although some papers stated that domain heights have been included in the final form of the proposed equations, the influence of domain height has not been fully understood yet. For that reason, this study only focuses on the effects of a domain height towards the distance in which a negative jet stream starts to detach from the top wall. Unlike the previous studies, the impinging negative jet in this study was in a weak regime using methods suggested by some literature, computational fluid dynamic simulation [3]-[7].

This study was done not only to predict spreading distance by manipulating the domain height but also will uncover the mystery inside the impinging negative jet flow behavior. Therefore, it can contribute to optimizing and supporting the betterment of practical applications of impinging negative jet. The smoke from the electrical welding GMAW can be diverted away from the welding operator's breathing area. The hot gas from the vertically taken-off airplane can be manipulated not to spread too widely to the airport buildings. The energy consumed by the air conditioners can be optimized if the conditioned air circulation is managed properly using the impinging negative jet principles.

2. Research Methods

This study was done in several stages to minimize errors that can potentially affect the accuracy of the final results. The first step was to prepare the computers for performing numerical simulations. After that, trial and error in modifying the programming codes that have been developed before for other types of flow so that an ideal condition for this study could be achieved. The next step was running computer simulations intensively followed by post-processing for the results of the simulation in order to observe the trend from the data.

A low Reynolds number was chosen, Re = 200, to make sure the jet stream was in the weak regime. The domain height chosen was around $8.8 \leq H/X_0 \leq 10.2$, and the Froude number chosen was adjusted with the domain height, Fr = 5.0. The Prandtl number was set similar to that in the literature, Pr = 7.0 in order to make the comparison study with previous research on the jet stream easy.

The study has been done numerically using several units of desktop PC which are connected using a gigabit ethernet switch and were run in parallel. The sketch of the numerical model for the jet flow is shown in Figure 3 (a). To optimize the available computer resources, numerical solution was done in two dimensional axisymmetric coordinates (2D). Some three-dimensional models were tested for validating the accuracy of two-dimensional models. The computational domain and the boundary conditions for the numerical models of the system can be seen in Figure 3 (b).

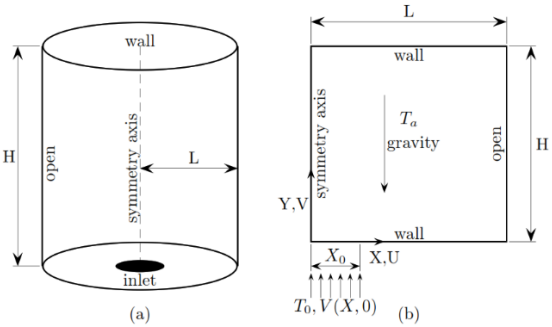

Figure 3. (a) Sketch of the system and (b) computational domain (This is drawn based on an illustration from Lin dan Armfield [4]).

The numerical approach applied in the study was solving Navier-Stokes equation directly. The equation has been modified to be non-dimensional and coupled with the energy equation to simulate density variation in the numerical model. The modified equation for the flow configuration in this study is written as follow,

$$\frac{1}{x}\frac{\partial}{\partial x}(xu) + \frac{\partial v}{\partial y} = 0 \quad (6)$$

$$\frac{\partial u}{\partial \tau} + \frac{1}{x}\frac{\partial}{\partial x}(xuu) + \frac{\partial}{\partial y}(uv) = -\frac{\partial p}{\partial x} + \frac{1}{Re}\left\{\frac{\partial}{\partial x}\left[\frac{1}{x}\frac{\partial}{\partial x}(xu)\right] + \frac{\partial^2 u}{\partial y^2} - \frac{u}{x^2}\right\} \quad (7)$$

$$\frac{\partial v}{\partial \tau} + \frac{1}{x}\frac{\partial}{\partial x}(xuv) + \frac{\partial}{\partial y}(vv) = -\frac{\partial p}{\partial y} + \left[\frac{1}{x}\frac{\partial}{\partial x}\left(x\frac{\partial v}{\partial x}\right) + \frac{\partial^2 v}{\partial y^2}\right] + \frac{1}{Fr^2\theta} \quad (8)$$

$$\frac{\partial \theta}{\partial \tau} + \frac{1}{x}\frac{\partial}{\partial x}(xu\theta) + \frac{\partial}{\partial y}(v\theta) = \frac{1}{RePr}\left[\frac{1}{x}\frac{\partial}{\partial x}\left(x\frac{\partial \theta}{\partial x}\right) + \frac{\partial^2 \theta}{\partial y^2}\right] \quad (9)$$

Where x is a horizontal axis and y is a vertical axis in which gravitation works. The velocity was made different depending on the direction in which u is the velocity in x-direction and v is the velocity in y-direction. Another variable used is p, that is pressure; θ is temperature and τ is time. All variables in the equation have been normalized so they are dimensionless.

Direct Numerical Simulation (DNS) technique was applied to solve the Navier-Stokes and the energy equations as written in (6) – (9) using the boundary conditions as illustrated in Figure 3. These equations were solved in a form of finite-volume on a non-staggered Cartesian grid. The spatial part of the differential equations was discretized by different methods, second-order and the ULTRA flux limiter. The advection part of the equation was solved using forward in time scheme of second-order Adams-Bashforth methods while the viscous of the equation was done by using Crank-Nicholson methods. Pressure correction methods, fractional-step were used to compel divergent free conditions and used to update the value of the pressure field. Rhie-Chow methods of momentum interpolation were used for calculating velocity on the cell face in the pressure solver. The equation system was then solved by using solver BI-CGSTAB with a Jacobi preconditioned multigrid. Detailed illustration on numerical methods used has been written in Ph.D. dissertation of Norris [15].

Some of the numerical techniques were then interpreted and written into programming codes using Fortran which were run in Debian Linux operating system. The Fortran used was Portland High Performance Fortran (PGHPF) version 12.0. The computer used was based on Intel CPU core i7-960 3.2 GHz which was one of intel microprocessor i-series first generation (Nehalem series 45 nm technology) This CPU consists of 4 cores with hyperthreading technology. Parallel computation was directly implemented in the programming codes both between cores in the same CPU and across different computers. There were about a total of 6 units of computers used in the simulations.

3. Result and Discussion

3.1 Stream visualization

The visualization of the typical flow behavior of an impinging jet with negative buoyancy force investigated in this study can be seen from the temperature contour plot at different time after the jet entered the domain as shown in Figure 4.

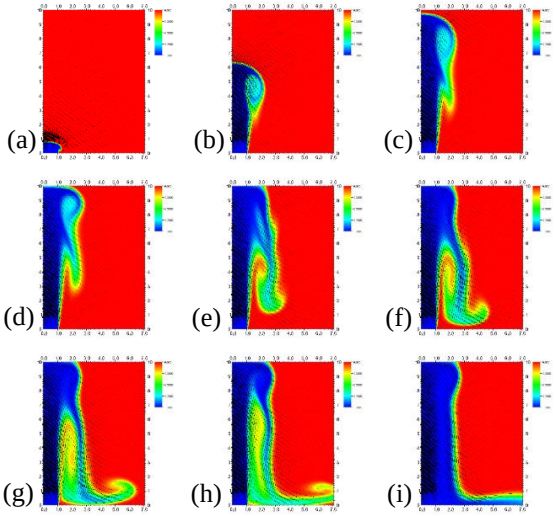

Figure 4. Flow visualization at Re = 200 (The number in every axis shows the domain relative size to the inlet)

The jet initially comes out from the inlet in fungus-like shape (Figure 4(a)). Then it moves further up until it reaches the top surface (Figure 4(b)-4(c)). Some parts of jet fluids went off from the flow and went down due to the influence of density differences with the fluids around. Some literature stated that the fungus-like form on the jet was caused by an entrainment phenomenon in which the ambient fluid was drawn by the jet movement [1, 2, 4, 8] and [9].

After hitting the ceiling (Figure 4(d)-4(f)), the jet then spreads along the surface until its momentum ends. After that, the jet fluid detaches from the top wall and falls down due to the negative buoyancy force. The falling fluid then mixes with the jet fluid that flows up to the ceiling. On the top part close to the ceiling, a big circulation flow was formed that is often called a recirculation area in the literature.

When the falling fluid reaches the domain base (Figure 4(g)), most of it will flow out but a few of it will be drawn back by the jet flow from the inlet forming a smaller recirculation area close to the bottom wall below the larger ones which is located near the ceiling. There is fluid trapped in the lower

recirculation area which is then slowly advected out and flows to the outlet of the domain before eventually getting out from the system (Figure 4(h)). The trapped fluid around causes relatively high-temperature differences between both upflow and downflow of the jet. The trapped fluid will slowly be advected out by the downflow until all parts of the jet flow both the up and down ones, will have the same temperature as the inlet temperature (Figure 4(i)).

3.2 Evolution of jet spreading distance

The distance of the jet flow detaching from the surface, X_d can be plotted against the time at various domain heights, H, in order to see its effect on X_d as shown in Figure 5. From the figure, it can be seen that the value of X_d will reach a maximum value before it then slowly decreases and reaches the final value at $\tau > 500$. The final value of the X_d X will then be used in linear regression analyses in the curve fitting process.

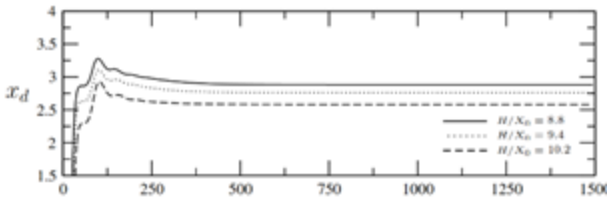

Figure 5. The evolution of jet spreading distance X_d against time at various H/X_0 (Obtained from post-processing of the simulation data.)

Figure 5 shows an identical pattern for each data at different heights. This has been predicted earlier as it is the same fluid and the same operating conditions. The difference is the jet with a shorter domain height will have a larger momentum when hitting a surface thus it will spread longer before detaching and falling down. The only equivocal difference is the jet with lower height $H/X_0 = 8.8$ will reach the final mark in a little bit longer of time, that is around $\tau > 500$, than $\tau > 400$ pada $H/X_0 = 9.4$ and $\tau > 250$ at $H/X_0 = 8.8$.

After the difference of the spreading distance X_d at various height H has been revealed, the comparison of the simulation result at different height H at final condition after reaching steady value needs to be further confirmed. The comparison of the jet flow was done at the domain heights of 8.8 and 9.8 using temperature contour plot as shown in Figure 6. It is clearly seen that there is a difference of the jet size especially in the recirculation area.

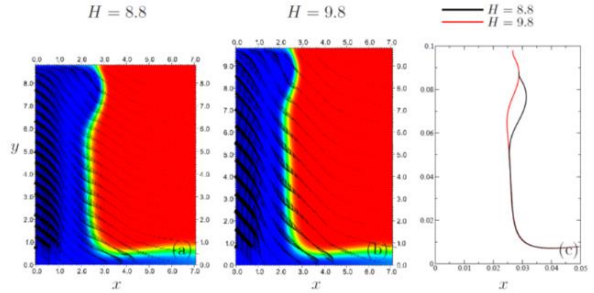

Figure 6. The comparison of simulation results (a) $H/X_0 = 8.8$ and (b) $H/X_0 = 9.8$. (c) iso profile temperature (Obtained from post-processing of the simulation data.)

In other parts, both jet flow profiles are basically identical as shown in Figure 6 as they were taken using the same operating condition. The difference was observed only in the recirculation area in which at $H/X_0 = 8.8$ the jet stream is wider and shorter because the size of the domain used is smaller. Other than the recisculation area, the line of iso profile temperature is identical one to another.

3.3 Curve fitting of the numerical data

From the evolution of the jet spreading distance X_d as shown in Figure 5, the final values after they become constant, X_{df} were then extracted for further analysis. A separate plot for X_{df} was created based on different H as shown in Figure 7.

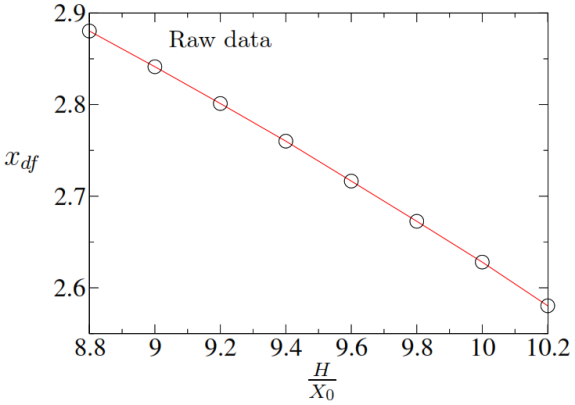

Figure 7 The raw data plot of the final spreading distance X_{df} against the domain height H/X_0. (Obtained from post-processing of the simulation data.)

From the *raw* data of X_{df} as shown in Figure 7, the influence of increasing H clearly showed a non-linear trend with the power value to be less than 1. As the exact pattern was difficult to obtain, the empical value was use instead. After rigorous searching by trial and error for several times, the most accurate result of the power with the highest possible accuracy for R^2 is $-\frac{1}{2}$. To get a better understanding of how accurate is the value of the chosen power for the whole range of H/X_0, the raw data is further processed and plotted together with the values of spreading distance X_{df} that are estimated using H/X_0 and the chosen power (Figure 8).

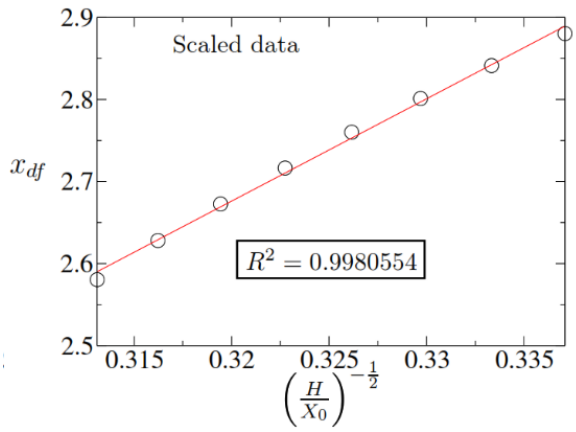

Figure 8. The scaled data plot of the final spreading distance X_{df} against the domain height H/X_0. (Obtained from post-processing of the simulation data.)

The data that is processed using the power of $-\frac{1}{2}$ is shown in small circle dots in the plot. Using linear regression analysis, the scaled data is then connected using a linear line. The linear regression equation of the line used in the curve fitting calculation is as follow,

$$x_{df} = -1.3169 + 12.478\left(\frac{H}{X_0}\right)^{-\frac{1}{2}} \quad (10)$$

As can be seen in Figure 8, the curve fitting process by using the power of $-\frac{1}{2}$ is accurate enough as all processed data lie on the regression line with an accuracy of $R^2 = 0.9980554$. The power of $-\frac{1}{2}$ in our study is actually similar to the power used in the equation suggested by Lemckert [13].

4. Conclusion

The effect of domain height to transient negative jet impinging on a rigid surface has been investigated numerically. The flow visualization obtained from the simulation results has successfully shown the flow pattern in detail. The unsteady behaviour of the jet has also been successfully studied. In addition, the existence of maximum spreading distance and different flow patterns at different domain heights have also been uncovered. There was a non-linear correlation for the domain height towards the final spreading distance. The regression equation with a power of $-\frac{1}{2}$ showed a good agreement with the data from the numerical simulation.

Reference

[1] L. J. Bloomfield and R. C. Kerr, Turbulent fountains in a stratified fluid, Journal of Fluid Mechanics, vol. 358, pp. 335-356, 1998.

[2] L. J. Bloomfield and R. C. Kerr, A theoretical model of a turbulent fountain , Journal of Fluid Mechanics, vol. 424, pp. 197-216, 2000.

[3] W. Lin and S. Armfield, Weak fountains in a stratified fluid, Physical Review, Vol 66, 066308, 2002.

[4] W. Lin and S. Armfield, Direct simulation of weak axisymmetric fountains in a homogeneous fluid, Journal of Fluid Mechanics, vol. 403, pp. 67-88, 2000.

[5] W. Lin and S. Armfield, The Reynolds and Prandtl number dependence of weak fountains, Computational Mechanics, vol. 31, pp. 379-389, 2003.

[6] W. Lin and S. Armfield, Direct simulation of fountains with intermediate Froude and Reynolds number, ANZIAM Journal, vol. 45(E), pp. C66-C77, 2004.

[7] W. Lin and S. Armfield, Onset of entrainment in transitional round fountains in a homogeneous fluid, International Journal of Heat and Mass Transfer, vol. 51, pp. 5226-5237, 2008.

[8] N. Williamson, S. W. Armfield and W. Lin, Transition behavior of weak turbulent fountains. Journal of Fluid Mechanics, vol. 655, pp. 306-326, 2010.

[9] N. Williamson, S. W. Armfield and W. Lin, Forced turbulent fountain flow behavior, Journal of Fluid Mechanics, vol. 671, pp. 535-558, 2011.

[10] K. Kuruppu and C. J. Lemckert, Plunging radius of water fountains following impact on a rigid surface, Proceedings of 7th Australasian Heat and Mass Transfer Conference, pp. 195-200, 2000.

[11] D. M. Holstein and C. J. Lemckert, Spreading of energetic submerged fountains impinging on a rigid surface, Proceedings of 14th Australasian Fluid Mechanics Conference, pp. 749-752, 2001.

[12] C. J. Lemckert, Spreading radius of fountains after impinging a free surface, Proceedings of 15th Australasian Fluid Mechanics Conference, pp. 217-220, 2004.

[13] C. J. Lemckert, Submerged fountains impinging on a smooth horizontal surface. Proceedings of 8th Australasian Heat and Mass Transfer Conference, pp. D10, 2005.

[14] P. Cooper and G. R. Hunt, Impinging axisymmetric turbulent fountains, Physics of Fluid, vol. 19, pp. 117101, 2007.

[15] S. E. Norris, A parallel Navier- Stokes solver for natural convection and free surface flow, PhD thesis, The University of Sydney, Australia, 2000.